

**Theoretical investigation of superconductivity in SrPd<sub>2</sub>Ge<sub>2</sub>, SrPd<sub>2</sub>As<sub>2</sub>, and CaPd<sub>2</sub>As<sub>2</sub>**Ertuğrul Karaca,<sup>1</sup> H. M. Tütüncü,<sup>1,2</sup> H. Y. Uzunok,<sup>1,2</sup> G. P. Srivastava,<sup>3</sup> and Ş. Uğur<sup>4</sup><sup>1</sup>*Sakarya Üniversitesi, Fen-Edebiyat Fakültesi, Fizik Bölümü, 54187, Adapazarı, Turkey*<sup>2</sup>*Sakarya Üniversitesi, BIMAYAM, Biyomedikal, Manyetik ve Yarıiletken Malzemeler Araştırma Merkezi, 54187, Adapazarı, Turkey*<sup>3</sup>*School of Physics, University of Exeter, Stocker Road, Exeter EX4 4QL, United Kingdom*<sup>4</sup>*Gazi Üniversitesi, Fen Fakültesi, Fizik Bölümü, Ankara, Turkey*

(Received 8 October 2015; revised manuscript received 7 December 2015; published 4 February 2016)

*Ab initio* pseudopotential calculations have been performed to investigate the structural, electronic, and vibrational properties of SrPd<sub>2</sub>Ge<sub>2</sub>, SrPd<sub>2</sub>As<sub>2</sub>, and CaPd<sub>2</sub>As<sub>2</sub> crystallizing in the ThCr<sub>2</sub>Si<sub>2</sub>-type body-centered tetragonal structure. Our electronic results show that the density of states at the Fermi level is mainly dominated by the strong hybridization of Pd *d* states and Ge (or As) *p* states. The linear response method and the Migdal-Eliashberg approach have been used to calculate the Eliashberg spectral function for all these compounds. By integrating the Eliashberg spectral function, the average electron-phonon coupling parameter ( $\lambda$ ) is found to be 0.74 for SrPd<sub>2</sub>Ge<sub>2</sub>, 0.66 for SrPd<sub>2</sub>As<sub>2</sub>, and 0.72 for CaPd<sub>2</sub>As<sub>2</sub>. Using the calculated values of  $\lambda$  and the logarithmically averaged phonon frequency  $\omega_{\text{lin}}$  the superconducting critical temperature ( $T_c$ ) values for SrPd<sub>2</sub>Ge<sub>2</sub>, SrPd<sub>2</sub>As<sub>2</sub>, and CaPd<sub>2</sub>As<sub>2</sub> are found to be 3.20, 2.05, and 2.48 K, respectively, which are in acceptable agreement with the corresponding experimental values. The relative differences in the  $T_c$  values between the Ge and As compounds have been explained in terms of some key physical parameters.

DOI: [10.1103/PhysRevB.93.054506](https://doi.org/10.1103/PhysRevB.93.054506)**I. INTRODUCTION**

ThCr<sub>2</sub>Si<sub>2</sub>-type  $AM_2X_2$  compounds (*A*: an alkaline earth or a lanthanide element; *M*: a transition metal; *X*: P, Ge, or As) have been extensively studied due to their interesting physical properties such as valence fluctuations and mixed valency [1,2]. Low temperature superconductivity has been found for LaRu<sub>2</sub>P<sub>2</sub> with a transition temperature ( $T_c$ ) of 4.1 K [3] while high temperature superconductivity has been discovered for Ba(K)Fe<sub>2</sub>As<sub>2</sub> with  $T_c$  as 38 K [4]. Some of the ThCr<sub>2</sub>Si<sub>2</sub>-type materials have been found to show different magnetic structures [5,6] while others undergo phase transition under pressure [7]. In 2009, the discovery of SrPd<sub>2</sub>Ge<sub>2</sub> as a new superconductor with  $T_c \sim 3$  K was reported in the experimental work of Fujii and Sato [8]. This discovery is very interesting because this material is pnictogen and chalcogen free. Moreover, due to the presence of the nonmagnetic metal Pd, no magnetic order exists to possibly weaken or interfere with the superconducting state. Following the experimental work of Fujii and Sato [8], the BCS-type superconductivity in SrPd<sub>2</sub>Ge<sub>2</sub> has been confirmed by different experimental groups [9–12]. Recently, the crystallographic, electronic transport, thermal, magnetic, and superconducting properties of SrPd<sub>2</sub>As<sub>2</sub> and CaPd<sub>2</sub>As<sub>2</sub> have been investigated in the experimental work of Anand and co-workers [13]. In this experimental study [13], the superconducting transition temperature values of  $T_c = 1.27$  K for CaPd<sub>2</sub>As<sub>2</sub> and  $T_c = 0.92$  K for SrPd<sub>2</sub>As<sub>2</sub> have been estimated from the zero-field  $C_p(T)$  data. These superconductors also provide an ideal playground to study the role of crystal structure for quenching magnetism and generating ambient pressure superconductivity.

The discovery of superconductivity in these and similar materials has motivated theoretical physicists to investigate their structural, elastic, and electronic properties. Shein and Ivanovskii [14] have investigated the structural and electronic properties of SrPd<sub>2</sub>Ge<sub>2</sub> by means of the first principles

full potential linearized augmented plane wave (FP-LAPW) method and the density functional theory (DFT). In this theoretical work the electronic band structure, total and partial density of states, and Fermi surface topology for SrPd<sub>2</sub>Ge<sub>2</sub> are calculated and discussed in comparison with those of the isostructural systems SrNi<sub>2</sub>Ge<sub>2</sub> and SrNi<sub>2</sub>As<sub>2</sub>. Moreover, this theoretical work has mentioned that the vibrational and electron-phonon interaction properties of SrPd<sub>2</sub>Ge<sub>2</sub> must be studied in order to explain the origin of its superconductivity. The FP-LAPW-DFT method has also been used to study the effect of pressure on the structural, electronic, and bonding properties of CaPd<sub>2</sub>As<sub>2</sub> in the work of Jayalakshmi and Sundareswari [15]. Pseudopotential plane-wave calculations [16], using DFT, are performed to investigate the structural, elastic, and thermodynamic properties of SrPd<sub>2</sub>Ge<sub>2</sub>. The first-principles calculations [17], using the FP-LAPW-DFT and pseudopotential-DFT as complementary approaches, are also used to investigate the elastic and electronic properties of CaPd<sub>2</sub>As<sub>2</sub> and SrPd<sub>2</sub>As<sub>2</sub>. Using a combination of these two theoretical techniques, Subedi and Singh [18] obtained  $T_c \sim 4$  K for BaNi<sub>2</sub>As<sub>2</sub>, which assumes the same crystal structure as SrPd<sub>2</sub>Ge<sub>2</sub>, SrPd<sub>2</sub>As<sub>2</sub>, and CaPd<sub>2</sub>As<sub>2</sub>. However, their theoretical estimate overestimates the experimental value of  $T_c = 0.7$  K [19]. Subedi and Singh explain this discrepancy possibly to arise from the lack of consideration of spin fluctuations in their theoretical treatment of the system.

Although some theoretical investigations of the structural and electronic properties of SrPd<sub>2</sub>Ge<sub>2</sub>, SrPd<sub>2</sub>As<sub>2</sub> and CaPd<sub>2</sub>As<sub>2</sub> have been presented, no experimental or theoretical results are available for the phonon dispersion relations and phonon density of states for these materials. In the absence of information regarding the phonon characteristics it is difficult to make an assessment of their phonon-related properties, such as specific heats, thermal expansion, and heat conduction. More importantly, in the present context, without good understanding of electron-phonon coupling it is difficult

to make a quantitative assessment of the superconducting properties of these materials.

In this paper, we have studied the structural and electronic properties of SrPd<sub>2</sub>Ge<sub>2</sub>, SrPd<sub>2</sub>As<sub>2</sub>, and CaPd<sub>2</sub>As<sub>2</sub> using the *ab initio* pseudopotential method based on a generalized gradient approximation of the density functional theory (DFT) [20]. The electronic band structure close to the Fermi energy is examined in detail. The phonon dispersion curves and density of states for these materials are calculated using a linear response theory [20]. The calculated phonon dispersion curves as well as the phonon density of states for these materials are compared between each other in detail. The linear response method [20] and the Migdal-Eliashberg approach [21,22] are used to determine the electron-phonon matrix elements for all the studied compounds. The phonon spectrum and the electron-phonon matrix elements are then used to obtain the Eliashberg spectral function [21–23], from which the electron-phonon coupling parameter is determined. Using the electron-phonon coupling parameter and the logarithmic average of phonon frequency, we finally compute the superconducting transition temperature.

## II. COMPUTATIONAL DETAILS

The calculations are carried out by means of the density functional theory with plane-wave expansion of the Kohn-Sham orbitals [24]. The exchange correlation functional is taken into account through the generalized gradient approximation (GGA) with the Perdew-Burke-Ernzerhof (PBE) functional [25]. Norm-conserving pseudopotentials [26] are used to treat the interaction of an ionic core and valence electrons. The following valence configurations are used in deriving the pseudopotentials: Sr (5s<sup>2</sup>, 5p<sup>0</sup>, 4d<sup>0</sup>), Ca (4s<sup>2</sup>, 4p<sup>0</sup>, 3d<sup>0</sup>), Pd (5s<sup>2</sup>, 5p<sup>0</sup>, 4d<sup>8</sup>), Ge (4s<sup>2</sup>, 4p<sup>2</sup>, 4d<sup>0</sup>), As (4s<sup>2</sup>, 4p<sup>3</sup>, 4d<sup>0</sup>). The electronic structure calculations have been carried out by solving the Kohn-Sham equation [24] and minimizing the total energy with respect to the relaxation of electrons, ions, and unit cell parameters in a self-consistent manner. The maximum kinetic energy cutoff for choosing the number of plane waves is chosen to be 60 Ry. Integration over the Brillouin zone (BZ) for total-energy calculations is performed by the Monkhorst-Pack scheme [27] using the 8 × 8 × 8 zone-centered grid, producing 59 *k* points in the irreducible part of the BZ (IBZ). The self-consistent electronic structure calculations are carried out by using the 24 × 24 × 24 zone-centered grid, producing 1063 *k* points in the IBZ.

Integration over the BZ for phonon calculations has been made by using the 8 × 8 × 8 grid (59 *k* points in the IBZ). The phonon frequencies and atomic displacements have been subsequently obtained using the linear response method [20], which refuses the use of supercell and allows the calculation of the dynamical matrix at arbitrary *q* vectors for phonons. Within the linear response scheme, second order derivatives of the total energy have been calculated to obtain the dynamical matrix. A static linear response of the valence electrons has been considered in terms of the variation of the external potential corresponding to periodic displacements of the atoms in the unit cell. The screening of the electronic system in response to the displacement of the atoms has been taken into account in a self consistent manner.

Integration up to the Fermi surface has been done with the smearing technique with the broadening parameter  $\sigma = 0.02$  Ry. We have calculated dynamical matrices at a uniform 4 × 4 × 4 grid of *q* points in the IBZ. Dynamical matrices at arbitrary wave vectors can be obtained by means of a Fourier deconvolution on this mesh. The technique for the calculation of the electron-phonon coupling has been well described in our previous work [28] and will not be repeated here. Fermi-surface sampling for the evaluation of the electron-phonon matrix elements has been done using the 24 × 24 × 24 *k* mesh with Gaussian of width 0.02 Ry. The phonon density of states and Eliashberg function have also been calculated for this *k* mesh.

## III. RESULTS

### A. Structural and electronic properties

All the considered APd<sub>2</sub>X<sub>2</sub> compounds crystallize in the body-centered tetragonal ThCr<sub>2</sub>Si<sub>2</sub>-type structure with the space group *I4/mmm*, which is displayed in Fig. 1. The atomic configuration contains one *A* atom at the (2*a*) (0, 0, 0) position, two Pd atoms at (4*d*) (0, 1/2, 1/4), and two *X* atoms at (4*e*) (0, 0, *z*). Thus, this tetragonal structure can be described by three parameters: two lattice parameters (*a* and *c*) and one internal parameter (*z*). The internal parameter *z* controls the Pd-X distance. The calculations have been made to find total energy results, which are then fitted into the Murnaghan equation of state to determine the structural parameters of the studied system. The calculated lattice parameters (*a* and *c*), the internal parameter (*z*), the closest Pd-X distance (*d*<sub>Pd-X</sub>), and

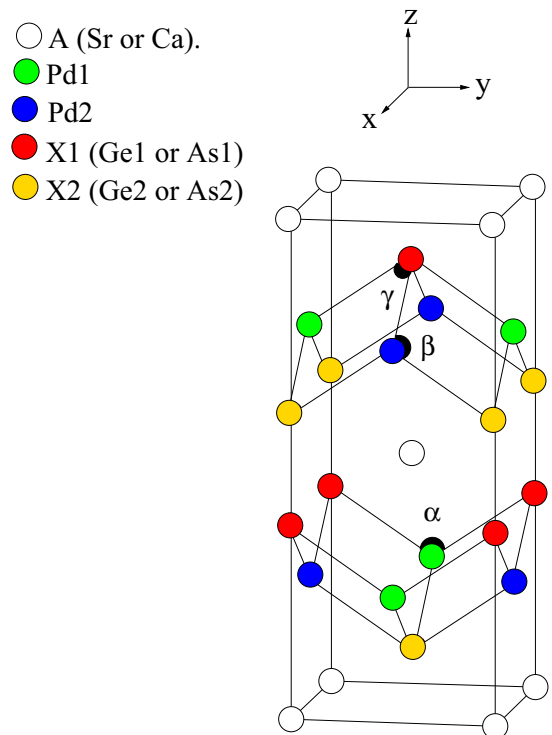


FIG. 1. The crystal structure of APd<sub>2</sub>X<sub>2</sub> showing X-Pd<sub>2</sub>-X-type layers and A ionic sheets alternatively stacked along the *c* axis.

TABLE I. Structural parameters for the body-centered tetragonal  $APd_2X_2$  ( $A = \text{Sr}$  or  $\text{Ca}$ , and  $X = \text{Ge}$  or  $\text{As}$ ), and their comparison with previous experimental and theoretical results.

Source	$a$ (Å)	$c$ (Å)	$z$	$d_{Pd-X}$ (Å)	$\alpha$	$\beta$	$\gamma$
SrPd <sub>2</sub> Ge <sub>2</sub>	4.423	10.259	0.372	2.542	120.85°	104.10°	75.90°
Experimental [8]	4.409	10.127	0.370	2.519	122.13°	103.54°	76.46°
Experimental [10]	4.420	10.104	0.370	2.521	122.49°	103.38°	76.62°
GGA [14]	4.459	10.321	0.370	2.573	121.34°	104.15°	76.12°
GGA [16]	4.373	9.981	0.370	2.493	122.58°	103.34°	76.66°
SrPd <sub>2</sub> As <sub>2</sub>	4.426	10.362	0.377	2.574	118.61°	105.11°	74.89°
Experimental [13]	4.376	10.167	0.377	2.539	118.99°	104.93°	75.07°
GGA [17]	4.437	10.364					
CaPd <sub>2</sub> As <sub>2</sub>	4.403	10.245	0.378	2.560	118.60°	105.11°	74.89°
Experimental [13]	4.282	10.088	0.376	2.492	118.48°	105.162°	74.84°
GGA [17]	4.357	10.247					

the bond angles ( $\alpha$ ,  $\beta$ , and  $\gamma$ ) are presented and compared with available experimental [8,10,13] and theoretical [14,16] results in Table I. The presently calculated lattice parameters  $a$  and  $c$  are, respectively, within 2.8% and 1.9% of their experimental values, and the calculated internal parameters are very close or equal to their experimental values. The values of the bond

angles  $\alpha$ ,  $\beta$ , and  $\gamma$  compare very well with their corresponding experimental values.

As can be seen from Table I, the replacement of Ca by the larger atom Sr causes to lengthen both of the lattice parameters  $a$  and  $c$  in SrPd<sub>2</sub>Ge<sub>2</sub> and SrPd<sub>2</sub>As<sub>2</sub>. The bond angles  $\alpha$ ,  $\beta$ , and  $\gamma$  are considerably different from the ideal tetrahedron angle

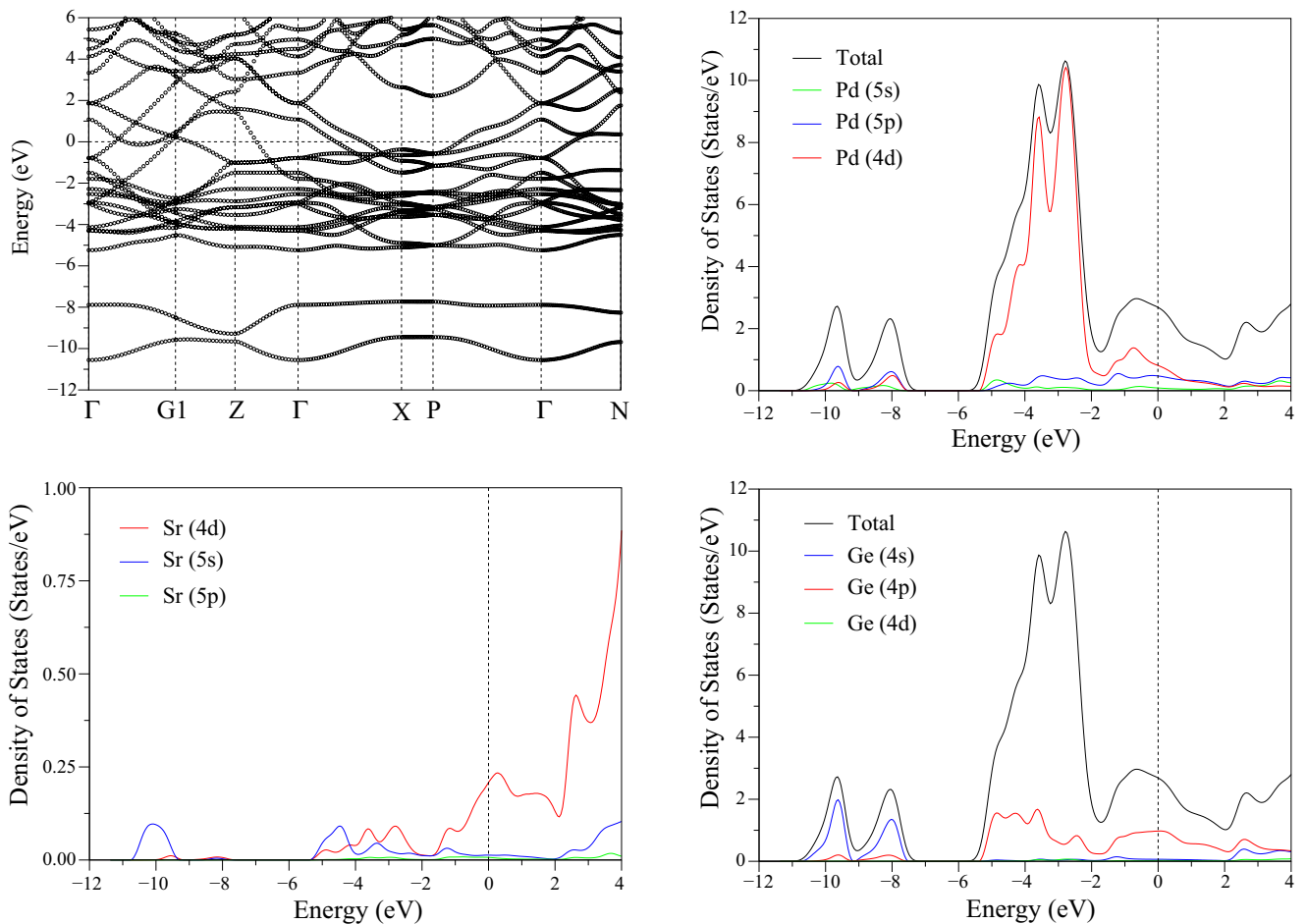


FIG. 2. The electronic band structure and density of states for SrPd<sub>2</sub>Ge<sub>2</sub>. The Fermi level corresponds to 0 eV. The high-symmetry points in the Brillouin zone in Cartesian coordinates are:  $G1 = \frac{2\pi}{a}((\frac{1}{2} + \frac{a^2}{2c^2}), 0.00, 0.00)$ ,  $Z = \frac{2\pi}{a}(0.00, 0.00, \frac{a}{c})$ ,  $X = \frac{2\pi}{a}(0.50, 0.50, 0.00)$ ,  $P = \frac{2\pi}{a}(0.50, 0.50, \frac{a}{2c})$ , and  $N = \frac{2\pi}{a}(0.0, 0.50, \frac{a}{2c})$ .

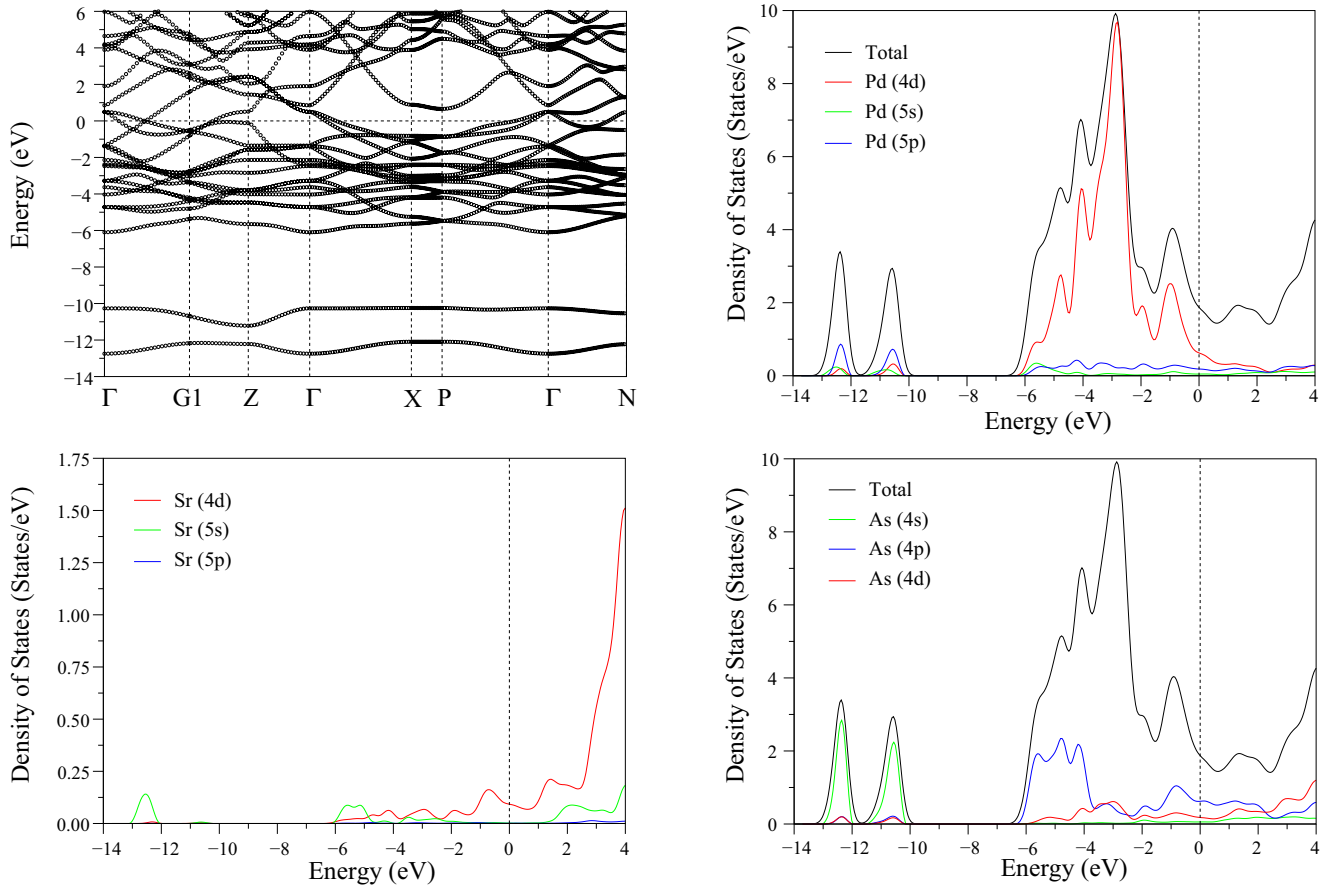


FIG. 3. The electronic band structure and density of states for SrPd<sub>2</sub>As<sub>2</sub>. The Fermi level corresponds to 0 eV.

value of  $109.5^\circ$  which is crucial for superconductivity in FeAs based superconductors [29–32]. The crystal structure of all the considered materials is formed by negatively charged [Pd<sub>2</sub>X<sub>2</sub>] layers and positively charged *A* layers, which alternately stack along the *c* axis. The role of the base metal component *A*, moreover, as its electron donor function is mainly a geometric one. Thus, the neighboring [Pd<sub>2</sub>X<sub>2</sub>] and *A* layers are coupled together due to ionic interactions. The atomic distances within the [Pd<sub>2</sub>X<sub>2</sub>] layers are slightly smaller than the sum of the corresponding atomic radii, which confirms a strong covalent bonding between Pd and X with some metallic character. Consequently, the overall bonding situation can be described as an interplay between covalent, metallic, and ionic interactions.

The electronic band structure, and total and partial density of states for SrPd<sub>2</sub>Ge<sub>2</sub> are displayed in Fig. 2. The overall band profile is in good agreement with previous theoretical results [14]. The electronic structure diagram proves the metallic property of this material since the metallic *d*-like bands, which are admixed with Ge *p* bands, cross the Fermi level. The two deep-lying bands in the intervals from  $-10.6$  to  $-9.6$  eV, and from  $-9.4$  to  $-7.8$  eV below the Fermi level consist of Ge 4*s* states and are separated by a gap of 2.5 eV from the higher valence band region, which extends from  $-5.5$  eV to the Fermi level. The energy levels in the range from  $-5.5$  to  $-2.0$  eV originate from Pd 4*d* states with considerable contributions from Ge 4*p* states. The contributions from the

valence states of Sr to these energy levels are quite small since these atoms are in the form of cations Sr<sup>2+</sup> and behave like electronic donors. The upper valence bands ( $-2$  to 0 eV) largely consist of hybridized Ge 4*p* and Pd 4*d* orbitals, confirming covalent Pd-Ge bonding. The value of density of states at the Fermi level [ $N(E_F)$ ] is calculated to be 2.70 states/eV which in good accordance with the previous GGA value of 2.90 states/eV [14]. The value of density of states at the Fermi level [ $N(E_F)$ ] is composed of approximately 8% Sr electronic states [ $N(E_F^{Sr}) = 0.216$  states/eV], 41% Pd electronic states [ $N(E_F^{Pd}) = 1.107$  states/eV], and 51% electronic states [ $N(E_F^{Ge}) = 1.377$  states/eV]. In particular, Ge 4*p* and Pd 4*d* states alone contribute to  $N(E_F)$  up to 36% and 30%, respectively. This observation shows that these electrons are most effective in developing the superconducting properties of SrPd<sub>2</sub>Ge<sub>2</sub>, since Cooper pairs in the BCS theory can be formed by electrons which have energies close to the Fermi level.

The electronic band structure along high symmetric directions, as well as the density of states, for SrPd<sub>2</sub>As<sub>2</sub> and CaPd<sub>2</sub>As<sub>2</sub> are illustrated in Figs. 3 and 4, respectively. The overall band profiles of both the materials are found to be in good agreement with previous theoretical results [17]. Again, Pd 4*d* and X 4*p* orbitals generate the main spectral weight in these two compounds. The two lowest bands related to As 4*s* states in these materials lie at lower energies than their corresponding Ge 4*s* bands in SrPd<sub>2</sub>Ge<sub>2</sub>. Thus, the closest

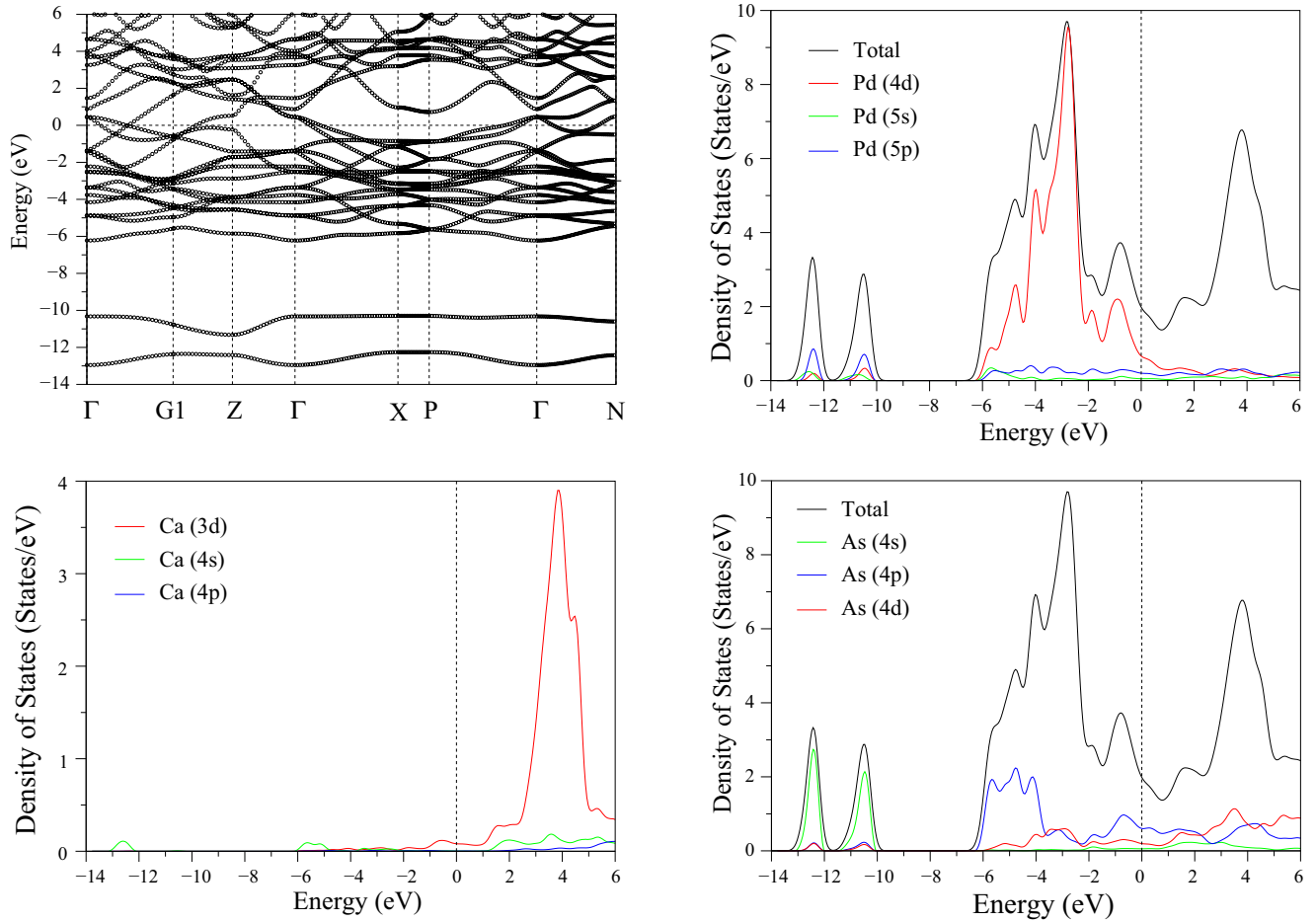


FIG. 4. The electronic band structure and density of states for  $\text{CaPd}_2\text{As}_2$ . The Fermi level corresponds to 0 eV.

As-As distance (around 2.53 Å) for these materials is shorter than the closet Ge-Ge distance (around 2.62 Å) for  $\text{SrPd}_2\text{Ge}_2$ . Secondly, the gap (around 4 eV) between two deep-lying bands and the main valence band region for these materials is 1.5 eV larger than the corresponding band gap for  $\text{SrPd}_2\text{Ge}_2$ . The main valence band region in these materials extends from -6.2 eV to the Fermi level. Thus, the main valence band region in these materials is extended as compared to  $\text{SrPd}_2\text{Ge}_2$ . When going from  $\text{SrPd}_2\text{Ge}_2$  to  $\text{SrPd}_2\text{As}_2$  (or  $\text{CaPd}_2\text{As}_2$ ), a considerable redistribution of the density of states near  $E_F$  is found. The value of density of states at the Fermi level is found to be 1.98 states/eV for  $\text{SrPd}_2\text{As}_2$  and 1.92 states/eV for  $\text{CaPd}_2\text{As}_2$ . The values of  $N(E_F^{Pd})$  and  $N(E_F^{As})$  for  $\text{SrPd}_2\text{As}_2$  ( $\text{CaPd}_2\text{As}_2$ ) are calculated to be 0.94 states/eV (0.93 states/eV) and 0.93 states/eV (0.90 states/eV) which are lower than the corresponding values for  $\text{SrPd}_2\text{Ge}_2$ . Thus, the total decrease in the value of  $N(E_F)$  for  $\text{SrPd}_2\text{As}_2$  and  $\text{CaPd}_2\text{As}_2$  can be linked to a decrease in the contributions from both the  $p$  states of  $X$  atoms and the  $d$  states of Pd atoms. The number of valence electrons in As is one more than that in Ge, and the Pd states in  $\text{SrPd}_2\text{As}_2$  and  $\text{CaPd}_2\text{As}_2$  are slightly extended in energy than the corresponding states in  $\text{SrPd}_2\text{Ge}_2$ ; as a result, the Fermi level in the compounds with As is shifted towards smaller densities of states.

## B. Phonons and electron-phonon interaction

We first examine the zone-center phonon modes in  $\text{APd}_2\text{X}_2$ , classified by the irreducible representations of the point group  $D_{4h}(4/mmm)$ . As obtained from group theory, the symmetries of the optical phonon modes are given as:

$$\Gamma = 2E_g + B_{1g} + 2E_u + 2A_u + A_{1g},$$

where the suffixes  $g$  and  $u$  represent even and odd parities, the one-dimensional  $A$  and  $B$  modes involve displacements along the  $z$  direction, and the doubly degenerate  $E$  modes represent displacement in the  $x$ - $y$  plane. The frequencies and electron-phonon coupling parameters of the zone-center optical phonon modes are presented in Table II. As can be seen from Table III, the largest electron-phonon coupling parameter for all the considered  $\text{APd}_2\text{X}_2$  compounds is found for the lower  $E_g$  phonon mode. The eigenvector representation of this phonon mode for  $\text{SrPd}_2\text{Ge}_2$  is illustrated in Fig. 5. This phonon mode is totally characterized by the vibrations of Pd and Ge atoms with Sr atoms at rest. This observation is expected since the largest contribution to the  $N(E_F)$  comes from the Pd  $d$  and Ge  $p$  states. The eigenvector representation of the  $E_g$  phonon mode dynamically causes changes on the tetrahedral bond angles in  $\text{PdGe}_4$ , which leads to the overlap of the Pd and Ge electronic states. This overlap generates the

TABLE II. Comparison of zone-center optical phonon frequencies (in THz) and their electron-phonon coupling parameters for SrPd<sub>2</sub>Ge<sub>2</sub>, SrPd<sub>2</sub>As<sub>2</sub>, and CaPd<sub>2</sub>As<sub>2</sub>.

Material	$E_g$	$E_u$	$B_{1g}$	$A_{2u}$	$A_{2u}$	$E_u$	$E_g$	$A_{1g}$
SrPd <sub>2</sub> Ge <sub>2</sub> ( $\nu$ )	1.867	3.285	3.312	3.762	5.146	5.702	5.779	5.847
SrPd <sub>2</sub> Ge <sub>2</sub> ( $\lambda$ )	0.154	0.006	0.077	0.005	0.009	0.004	0.026	0.143
SrPd <sub>2</sub> As <sub>2</sub> ( $\nu$ )	0.974	3.151	2.366	3.545	4.451	5.087	5.489	6.201
SrPd <sub>2</sub> As <sub>2</sub> ( $\lambda$ )	0.621	0.004	0.092	0.005	0.005	0.006	0.026	0.122
CaPd <sub>2</sub> As <sub>2</sub> ( $\nu$ )	0.861	3.765	2.201	4.290	4.603	5.245	5.619	6.807
CaPd <sub>2</sub> As <sub>2</sub> ( $\lambda$ )	0.734	0.004	0.111	0.008	0.003	0.006	0.027	0.101

larger electron-phonon coupling parameter for the  $E_g$  phonon mode than other zone-center phonon modes. The value of electron-phonon coupling parameter for the lower  $E_g$  phonon mode is found to be 0.62 and 0.73 for SrPd<sub>2</sub>As<sub>2</sub> and CaPd<sub>2</sub>As<sub>2</sub>, respectively. These values are higher than the corresponding value for SrPd<sub>2</sub>Ge<sub>2</sub> in accordance with the McMillan-Hopfield expression, according to which the electron-phonon coupling parameter can be given as

$$\lambda = \frac{N(E_F)\langle I^2 \rangle}{M\langle \omega^2 \rangle}, \quad (1)$$

where  $\langle I^2 \rangle$  shows the averaged square of the electron-phonon matrix element,  $\langle \omega^2 \rangle$  is the averaged square of the phonon frequency, and  $M$  is the mass involved. While  $N(E_F)$  is bigger for SrPd<sub>2</sub>Ge<sub>2</sub>, due to the much softer  $E_g$  phonon mode the ratio  $N(E_F)/\omega^2$  is bigger in the APd<sub>2</sub>As<sub>2</sub> compounds.

In order to gain full understanding of the role of phonons in the BCS superconductivity of these materials, we present and examine the phonon dispersion curves, phonon density of states, the Eliashberg spectral function, and the electron-phonon coupling constant along the high symmetry lines in the Brillouin zone. The primitive cell of the body-centered tetragonal SrPd<sub>2</sub>Ge<sub>2</sub> material contains one formula unit with the total of five atoms, leading to a total of 15 phonon branches (three acoustic and twelve optical). The calculated phonon dispersion relations for SrPd<sub>2</sub>Ge<sub>2</sub> are shown in Fig. 6(a). The

TABLE III. Comparison of superconducting state parameters for SrPd<sub>2</sub>Ge<sub>2</sub>, SrPd<sub>2</sub>As<sub>2</sub>, and CaPd<sub>2</sub>As<sub>2</sub>. The parameter  $\mu^*$  is taken to be 0.13.

Material	$N(E_F)$ (States/eV)	$\omega_{ln}$ (K)	$\lambda$	$T_C$ (K)	$\gamma$ ( $\frac{mJ}{molK^2}$ )
SrPd <sub>2</sub> Ge <sub>2</sub>	2.70	101.4	0.74	3.20	11.04
Experimental [8]				3.04	
Experimental [9]				2.70	7.83
Experimental [11]				2.92	15.3
Experimental [12]				2.90	
GGA [14]	2.90				6.84
SrPd <sub>2</sub> As <sub>2</sub>	1.98	92.2	0.66	2.05	7.71
Experimental [13]			0.44	0.92	6.43
GGA [17]	1.97				4.65
CaPd <sub>2</sub> As <sub>2</sub>	1.92	84.29	0.72	2.48	7.82
Experimental [13]	1.87		0.47	1.27	6.52
GGA [17]	1.86				4.40

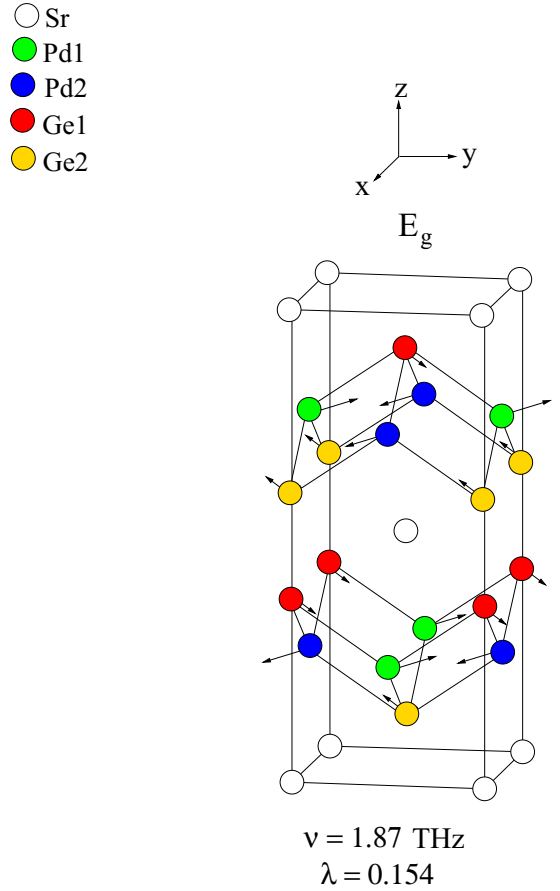


FIG. 5. An schematic illustration of the eigendisplacements pattern of the lower  $E_g$  phonon mode for SrPd<sub>2</sub>Ge<sub>2</sub>.

phonon spectrum can be separated into two clear regions: a low frequency region (LFR) from 0 to 3.8 THz and a high frequency region (HFR) in the frequency ranges of 4.6 to 5.9 THz. The separation of 0.8 THz between the two frequency regions results from the mass difference between different types of atoms. The LFR is comprised of the three acoustic and six optical branches extending up to 3.8 THz. All phonon branches in this region are dispersive and there is significant overlap between the acoustic and optical branches. The HFR consists of six optical branches. The highest optical phonon branch is weakly dispersive compared to the other optical phonon branches in this frequency region.

The calculated total phonon density of states and the partial phonon density of states of atoms of different type are presented in Fig. 6(b). A strong hybridization of Pd and Ge atoms dominates the density of states features in the frequency region from 0 to 2.2 THz. In the frequency range 2.2 to 2.7 THz, the main contribution to the density of states comes from the vibrations of Pd atoms with smaller contribution of remaining atoms. The frequency region from 2.7 to 3.8 THz is mainly derived from Sr atoms with smaller contribution of remaining atoms. Above the gap region, the density of states features are mainly characterized by the motions of Ge atoms due to their light mass. Although Pd atoms are the heaviest of three type atoms, they make significant contribution to the density of states in the HFR, while Sr atoms remain relatively

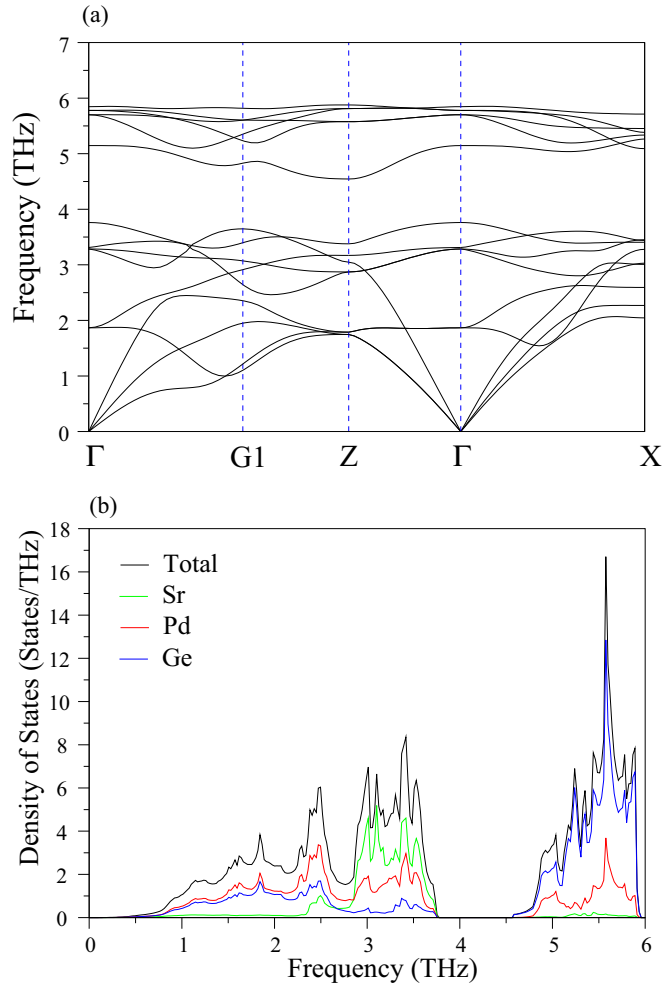


FIG. 6. (a) The calculated phonon dispersion curves along high symmetry directions in the Brillouin zone for the body-centered tetragonal  $\text{SrPd}_2\text{Ge}_2$ . (b) Total and partial phonon density of states for  $\text{SrPd}_2\text{Ge}_2$ .

silent. These considerable contributions from Ge and Pd can be linked to the strong covalent bond between these atoms.

The calculated phonon dispersion curves along the high symmetry directions of the Brillouin zone, together with PDOS, for  $\text{SrPd}_2\text{As}_2$  are shown in Fig. 7. We have to note that the phonon spectra for  $\text{SrPd}_2\text{As}_2$  looks different from that for  $\text{SrPd}_2\text{Ge}_2$  (see also Fig. 6). A critical assessment of the phonon dispersion curves reveals that there are four frequency regions in which phonon bands distributed. Again there are three acoustic and six optical bands extending up to 3.6 THz in the first frequency region and the acoustic modes disperse up to around 3 THz in this frequency region. In the frequency range from 4.2 to 4.6 THz, there is only one optical phonon band which is separated by a small gap of 0.3 THz from the four optical phonon branches distributed in the frequency range from 4.9 to 5.5 THz. Finally, the highest surface optical phonon branch is separated from these four optical phonon branches by a gap of 0.4 THz. The critical assessment of the PDOS for  $\text{SrPd}_2\text{As}_2$  shows that the low frequency region below 2.0 THz consists of the acoustical and optical vibrations of Pd and As atoms with negligible contributions coming from Sr

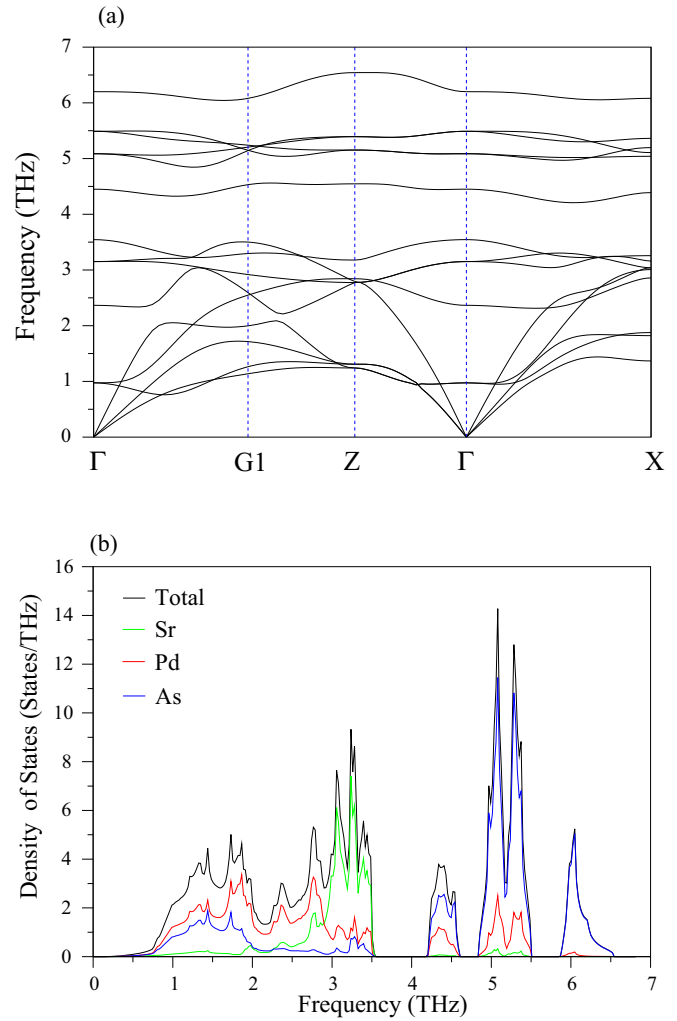


FIG. 7. (a) The calculated phonon dispersion curves along high symmetry directions in the Brillouin zone for the body-centered tetragonal  $\text{SrPd}_2\text{As}_2$ . (b) Total and partial phonon density of states for  $\text{SrPd}_2\text{As}_2$ .

atoms. The frequency region from 2.0 to 2.8 THz comes from the coupled motion of all atoms with maximum contribution coming from Pd atoms due to their heavy mass. The PDOS shows a dominance of Sr atoms in the frequency region from 2.8 THz to 3.6 THz with much smaller contributions from the remaining atoms. Above 3.6 THz, the contribution of As atoms to the PDOS features is largest due to their lightest mass.

The calculated phonon dispersion curves along the high symmetry directions of the Brillouin zone, together with total and partial density of states, for  $\text{CaPd}_2\text{As}_2$  are shown in Fig. 8. The full phonon spectrum has a frequency range of about 7.1 THz, which is larger than that for  $\text{SrPd}_2\text{Ge}_2$  (5.9 THz) and  $\text{SrPd}_2\text{As}_2$  (6.6 THz). Different from the other materials, the three acoustic and three optical phonon branches form a low frequency region below 3.3 THz, while the second frequency region from 3.6 to 4.3 THz is generated by three Ca-related optical phonon branches. A gap region of around 0.3 THz separates these two regions from each other. In the third frequency region, from 4.4 to 4.8 THz, there is only one optical phonon band which is separated by a very small gap

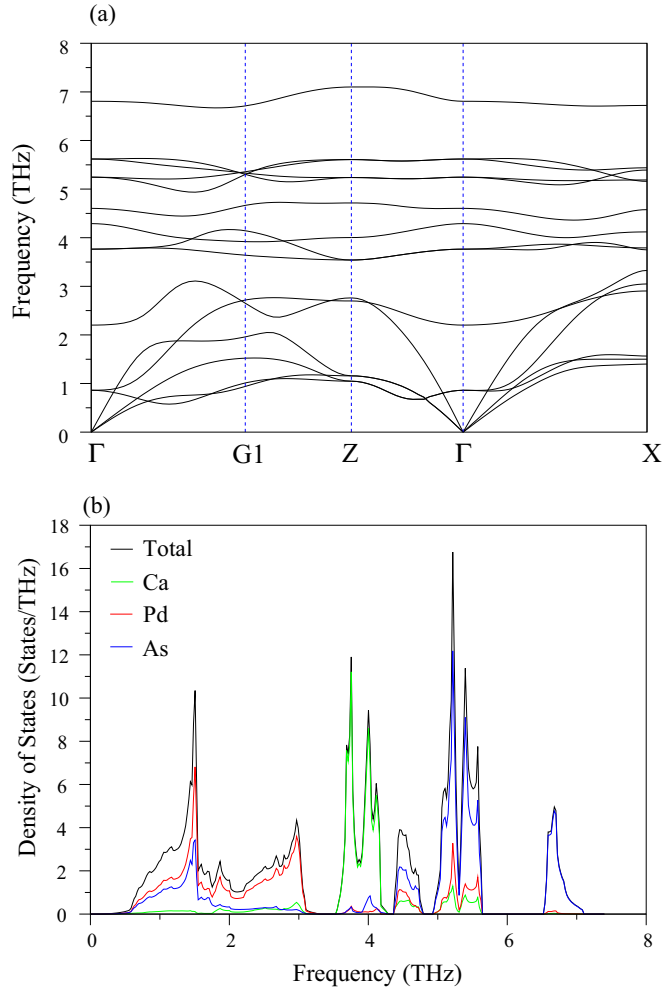


FIG. 8. (a) The calculated phonon dispersion curves along high symmetry directions in the Brillouin zone for the body-centered tetragonal  $\text{CaPd}_2\text{As}_2$ . (b) Total and partial phonon density of states for  $\text{CaPd}_2\text{As}_2$ .

of 0.1 THz from the four optical phonon branches distributed in the fourth frequency region from 4.9 to 5.7 THz. Similar to what was noticed in  $\text{SrPd}_2\text{As}_2$ , the fourth region includes only the highest surface optical mode which disperses from 6.5 to 7.1 THz. From a critical assessment of the partial density of states, we have observed that Pd, the heaviest element, provides the dominant contribution in the low frequency range of 0–3.3 THz. In the frequency range of 0–1.8 THz, a considerable Pd-As hybridization can be seen. Further, a much smaller Ca contribution has been observed in this lower frequency range of 0–3.3 THz. However, the contribution of Ca to the phonon modes is strongest between 3.6 and 4.3 THz. Different from  $\text{SrPd}_2\text{Ge}_2$  and  $\text{SrPd}_2\text{As}_2$ , the A atoms (Ca atoms) make considerable contributions to the higher frequency region due to the smaller mass of Ca as compared to that of Sr. Thus, the frequency region from 4.4 to 5.7 THz arises from the coupled motion of all atoms, but the maximum contribution comes from As atoms. Finally, the highest surface optical phonon mode creates a peak at 6.7 THz.

The Eliashberg spectral function ( $\alpha^2F(\omega)$ ) for  $\text{SrPd}_2\text{Ge}_2$ ,  $\text{SrPd}_2\text{As}_2$ , and  $\text{CaPd}_2\text{As}_2$  are presented in Fig. 9. In general,

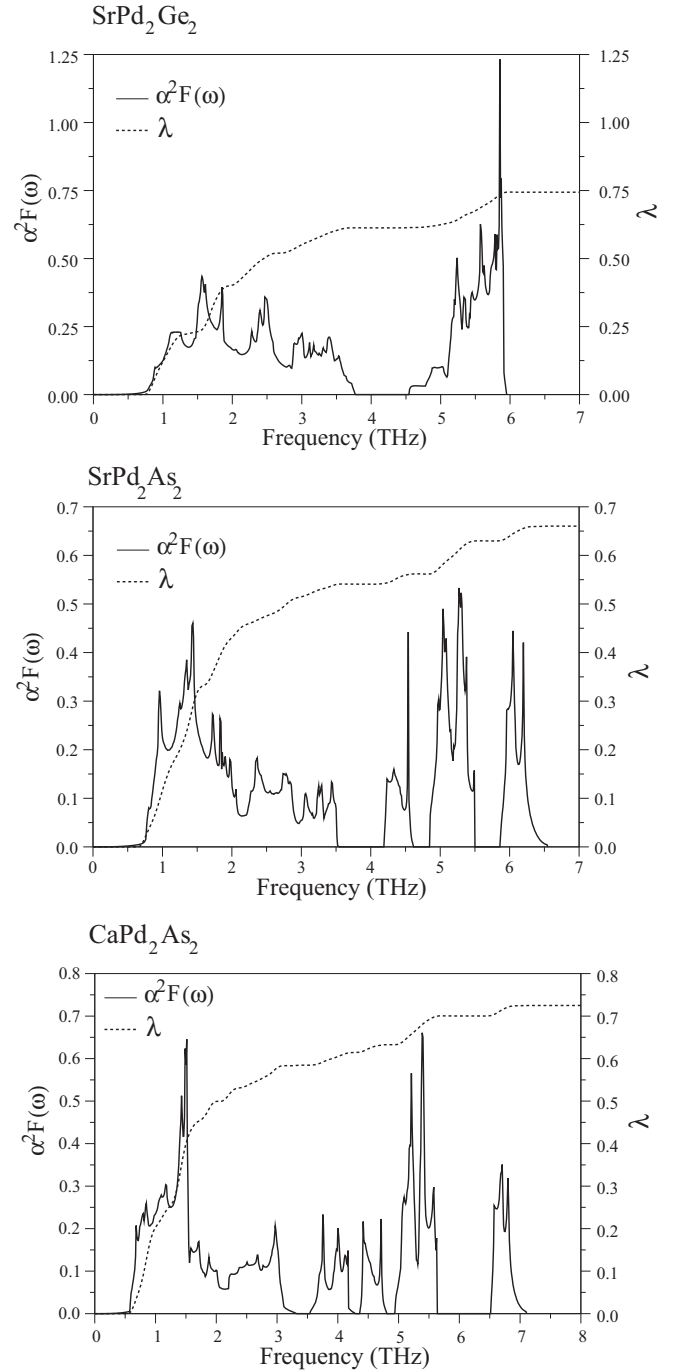


FIG. 9. The calculated electron-phonon spectral function  $\alpha^2F(\omega)$  (solid line) and the accumulative electron-phonon coupling parameter  $\lambda$  (dashed line) for  $\text{APd}_2\text{X}_2$  superconductors.

the Eliashberg spectral function follows the structure of the phonon density of states in the frequency space. We can further calculate frequency dependent electron-phonon coupling constant  $\lambda(\omega) = \frac{\alpha^2F(\omega)}{\omega}$  and frequency accumulative electron-phonon coupling constant  $\lambda_{\text{acc}} \equiv \lambda = 2 \int \frac{\alpha^2F(\omega)}{\omega} d\omega$ . We find that the accumulative electron-phonon coupling parameter ( $\lambda_{\text{acc}}$ ) is equal to 0.74 for  $\text{SrPd}_2\text{Ge}_2$ , 0.66 for  $\text{SrPd}_2\text{As}_2$  and 0.72 for  $\text{CaPd}_2\text{As}_2$ , indicating clearly that  $\text{SrPd}_2\text{Ge}_2$  and  $\text{CaPd}_2\text{As}_2$



are more likely to show superconductivity with a higher superconducting critical temperature ( $T_c$ ) than SrPd<sub>2</sub>As<sub>2</sub>.

The accumulative coupling parameter  $\lambda$  for SrPd<sub>2</sub>Ge<sub>2</sub> increases strongly with rising frequency in the range 0.0 to 3.8 THz. The phonon bands in this region contribute about 82% (0.61) to  $\lambda$  while the contribution of phonon branches between 4.6 and 5.9 THz contribute only about 18% (0.13). In general, a similar observation has been made for the other two materials. Thus, we can conclude that acoustic as well as low-frequency optical phonon branches due to the coupled motion of Pd and X (Ge or As) atoms are strongly involved in the process of scattering of electrons than the phonon modes with high frequency. This conclusion is expected because of the considerable contributions of the Pd  $d$  and X (Ge or As)  $p$  states at the Fermi energy in APd<sub>2</sub>X<sub>2</sub>.

The electron-phonon coupling constant  $\lambda$  also contributes to the electronic specific heat coefficient  $\gamma$ , which is renormalized by the ‘‘phonon enhancement’’ factor  $(1 + \lambda)$  compared to its ‘‘band structure’’ value:

$$\begin{aligned} \gamma_{\text{renorm}} &= \gamma_{\text{bs}}(1 + \lambda), \\ &= \frac{1}{3}\pi^2 k_B^2 N(E_F)(1 + \lambda). \end{aligned} \quad (2)$$

Using the average electron-phonon coupling constant  $\lambda$  and the logarithmically averaged phonon frequency  $\omega_{\text{ln}}$

$$\omega_{\text{ln}} = \exp\left(2\lambda^{-1} \int_0^\infty \frac{d\omega}{\omega} \alpha^2 F(\omega) \ln \omega\right), \quad (3)$$

the superconducting transition temperature  $T_c$  is computed from the Allen-Dynes modification of the McMillian formula [23]

$$T_c = \frac{\omega_{\text{ln}}}{1.2} \exp\left(-\frac{1.04(1 + \lambda)}{\lambda - \mu^*(1 + 0.62\lambda)}\right), \quad (4)$$

where  $\mu^*$  is an effective screened Coulomb repulsion constant. The value of  $\mu^*$  is chosen to be 0.13 for all the APd<sub>2</sub>X<sub>2</sub> compounds studied here. The calculated values of  $N(E_F)$ ,  $\omega_{\text{ln}}$ ,  $\lambda$ ,  $T_c$ , and  $\gamma$  are presented in Table III. Our results are also compared with previous experimental [8,9,11–13] and theoretical results [14,17] in this table. In general, the presently calculated superconducting parameters for all the presently studied materials are in reasonable accordance with available experimental [8,9,11–13] and theoretical results [14,17]. In particular, the calculated  $T_c$  value of 3.20 K for SrPd<sub>2</sub>Ge<sub>2</sub> is in perfect agreement with its experimental value [8] of 3.04.

The density of states at the Fermi level [ $N(E_F)$ ], the logarithmic average phonon frequency  $\omega_{\text{ln}}$ , and the strength of electron-phonon coupling parameter  $\lambda$  may effect the  $T_c$  values of BCS-type superconductors according to the McMillan-Hopfield and the Allen-Dynes modified McMillian equations. As regards the electronic structure, the largest  $N(E_F)$  value is obtained for SrPd<sub>2</sub>Ge<sub>2</sub>. Moreover, the values of  $\lambda$  and  $\omega_{\text{ln}}$  for SrPd<sub>2</sub>Ge<sub>2</sub> are larger than the corresponding values for SrPd<sub>2</sub>As<sub>2</sub> and CaPd<sub>2</sub>As<sub>2</sub>. Thus, we can safely conclude that the  $T_c$  value of SrPd<sub>2</sub>Ge<sub>2</sub> is larger than those of SrPd<sub>2</sub>As<sub>2</sub> and CaPd<sub>2</sub>As<sub>2</sub>. In order to understand the role of phonons directly via the logarithmic average  $\omega_{\text{ln}}$  and indirectly via the electron-phonon coupling parameter  $\lambda$  we express Eq. (4) as

$$T_c = \frac{\omega_{\text{ln}}}{1.2} \exp[-\eta], \quad (5)$$

where  $\eta = \frac{1.04(1+\lambda)}{\lambda - \mu^*(1+0.62\lambda)}$ . Our numerical results suggest that  $\eta[\text{CaPd}_2\text{As}_2]$  is 30% lower than  $\eta[\text{SrPd}_2\text{As}_2]$ , and  $\eta[\text{SrPd}_2\text{Ge}_2]$  is 39% lower than  $\eta[\text{SrPd}_2\text{As}_2]$ . On the other hand,  $\omega_{\text{ln}}[\text{CaPd}_2\text{As}_2]$  is 9% lower than  $\omega_{\text{ln}}[\text{SrPd}_2\text{As}_2]$ , and  $\omega_{\text{ln}}[\text{SrPd}_2\text{As}_2]$  is 10% lower than  $\eta[\text{SrPd}_2\text{Ge}_2]$ . It is clear that the indirect role of phonons, via the  $\eta$  (or  $\lambda$ ) factor, is dominant over their direct role via  $\omega_{\text{ln}}$ .

#### IV. DISCUSSION AND SUMMARY

In this paper, we have studied the structural, electronic, vibrational, and superconducting properties of APd<sub>2</sub>X<sub>2</sub> ( $A = \text{Sr, Ca}$  and  $X = \text{Ge, As}$ ) crystallized in the body centered tetragonal ThCr<sub>2</sub>Si<sub>2</sub> type of crystal structure by using the generalized gradient approximation of the density functional theory and the plane-wave pseudopotential method. The calculated structural parameters for all the studied compounds are in good accordance with existing theoretical and experimental results. Our calculated electronic structures compare very well with available theoretical electronic structures, and clearly show the metallic nature of these materials. The bonding in these compounds can be described as a mixture of metallic, ionic, and covalent contributions.

An examination of the Eliashberg spectral function  $\alpha^2 F(\omega)$ , based on our calculated phonon dispersion curves and density of states, shows that in all the considered APd<sub>2</sub>X<sub>2</sub> materials the acoustic as well as low-frequency optical phonon modes, rather than high frequency optical phonon modes, are heavily involved in the process of scattering electrons near the Fermi level. These active phonon modes are dominated by the hybridization of Pd and X vibrations, and the electronic states of these atoms make huge contributions to the density of states at the Fermi level. From the integration of Eliashberg spectral function, the average electron-phonon coupling parameter is found to be 0.74 for SrPd<sub>2</sub>Ge<sub>2</sub>, 0.66 for SrPd<sub>2</sub>As<sub>2</sub> and 0.72 for CaPd<sub>2</sub>As<sub>2</sub>. This result suggests that the electron-phonon interaction in SrPd<sub>2</sub>Ge<sub>2</sub> is slightly stronger than the corresponding interaction in its isostructural compounds SrPd<sub>2</sub>As<sub>2</sub> and CaPd<sub>2</sub>As<sub>2</sub>. The larger value of  $\lambda$  for SrPd<sub>2</sub>Ge<sub>2</sub> can be linked to its large density of states at the Fermi level [ $N(E_F)$ ]. Thus, we can state that all the studied compounds are phonon-mediated superconductors with the medium electron-phonon coupling strength.

Using the Allen-Dynes modified McMillian equation with the screened Coulomb pseudopotential parameter  $\mu^* = 0.13$ , the superconducting critical temperature is calculated to be 3.20 K for SrPd<sub>2</sub>Ge<sub>2</sub>, 2.05 K for SrPd<sub>2</sub>As<sub>2</sub>, and 2.48 K for CaPd<sub>2</sub>As<sub>2</sub>. These are in admissible accordance with their corresponding experimental values. Equation (5) suggests that there are two factors that determine  $T_c$ . Higher values of the logarithmic average of phonon frequencies  $\omega_{\text{ln}}$  is directly indicative of linearly increasing value of  $T_c$ . The electron-phonon coupling constant  $\lambda$  provides an indirect but exponentially strong reduction in  $T_c$  through its relationship with the parameter  $\eta$ . Larger values of the coupling parameter  $\lambda$ , in turn, result from concomitant presence of larger  $N(E_F)$  and smaller averaged square of the phonon frequency. The logarithmic average of phonon frequencies  $\omega_{\text{ln}}$  for SrPd<sub>2</sub>Ge<sub>2</sub> is only about 10% lower than that for SrPd<sub>2</sub>As<sub>2</sub>. However,

$\eta(\text{Ge})$  is about 39% lower than  $\eta(\text{As})$ . Thus, the indirect role of  $\lambda$  (or  $\eta$ ) dominates over the direct role of  $\omega_{\text{ln}}$  in making  $T_c(\text{Ge})$  larger than  $T_c(\text{As})$ .

Previous *ab initio* works have reported much higher values of  $T_c$  than the corresponding experimental measurements. These include the work by Subedi and Singh [18] on  $\text{BaNi}_2\text{As}_2$ , the work by Ortenzi *et al.* [33] on  $\text{CuBiSO}$ , and the work by Subedi [34] on  $\text{K}_2\text{Cr}_3\text{As}_3$ . As noted in Table III that there are four estimates of  $T_c$  from experimental studies on  $\text{SrPd}_2\text{Ge}_2$  in Refs. [8] and [9]: these range from 2.70 K to 3.04 K. Our theoretical result of 3.20 K is higher than the average of the four experimental results (2.89 K). In contrast, there seems to be only a single experimental result for each of the other two materials. Our theoretical estimate is much higher for these two materials. Further experimental studies may become necessary before we conclude that there is 100% (or more) theoretical overestimation of  $T_c$  for these two materials. What is intriguing is that there is reasonably good agreement between theory and experiment for  $\lambda$  and  $\gamma$  for  $\text{SrPd}_2\text{As}_2$  and  $\text{CaPd}_2\text{As}_2$ . This is in almost total contrast to the results for  $\gamma$  for  $\text{SrPd}_2\text{Ge}_2$ , where the theoretical value of  $11.04 \frac{\text{mJ}}{\text{molK}^2}$  lies between the two widely different experimental results of  $7.83 \frac{\text{mJ}}{\text{molK}^2}$  and  $15.3 \frac{\text{mJ}}{\text{molK}^2}$ .

Several possible reasons have been suggested for theoretical overestimation of  $T_c$  in these materials. The most plausible is the presence of spin fluctuation. Other possibilities include nonstoichiometric (dirty/doped) samples used in experimental measurements, uncertainty in the calculation of  $\lambda$  using the linear-response approximation and the subsequent calculation of  $T_c$  using the simplified Allen-Dynes formula, and the neglect of phonon anharmonicity. It is our view that the last two issues are unlikely to make a huge difference in the theoretical estimate of  $T_c$  using the simplified Allen-Dynes formula, and the neglect of phonon anharmonicity. It is therefore important to investigate the role of spin fluctuations and sample nonstoichiometry on  $T_c$ . Both of these issues are challenging. Investigation of nonstoichiometric effects will be limited by computational facilities. On the other hand, studies of spin fluctuations cannot be adequately dealt with the standard DFT formalism. This is because DFT calculations, which usually deal with nondynamic states, produce a magnetic (rather than paramagnetic) ground state. Although not attempted in this

work, DFT calculations with spin-polarized states or with spin-orbit interactions included, should be worth undertaking in future calculations to investigate their role in changing theoretical estimates of  $T_c$ . More experimental studies using samples with different stoichiometry would also be very helpful in this respect.

## V. CONCLUSION

Our *ab initio* investigations reveal that  $\text{SrPd}_2\text{Ge}_2$ ,  $\text{SrPd}_2\text{As}_2$ , and  $\text{CaPd}_2\text{As}_2$  crystallizing in the  $\text{ThCr}_2\text{Si}_2$ -type body-centered tetragonal structure are BCS-type superconductors with the medium-range values of the electron-phonon coupling parameter  $\lambda$  of 0.74, 0.66, and 0.72, respectively. Using the calculated values of  $\lambda$  and the logarithmically averaged phonon frequency  $\omega_{\text{ln}}$  the superconducting critical temperature ( $T_c$ ) values for these compounds are calculated to be 3.20, 2.05, and 2.48 K, respectively. These values are consistently much higher than reported experimental values. Some possible explanation for the theoretical overestimation of  $T_c$  has been forwarded. Notwithstanding such theoretical-experimental discrepancies, our work explains that the higher  $T_c$  result for the Ge compound compared to the As compounds in terms of two physical parameters: larger logarithmic average of phonon frequencies ( $\omega_{\text{ln}}$ ) and larger electron-phonon coupling constant ( $\lambda$ ). It is further pointed out the while  $\omega_{\text{ln}}$  makes a direct but smaller effect,  $\lambda$  makes an indirect but stronger effect in establishing the relative contributions towards  $T_c$ . Some suggestions have been made further theoretical and experimental studies for examining the consistently large difference between the theoretical and experimental values of  $T_c$ .

## ACKNOWLEDGMENTS

This work was supported by the Scientific and Technical Research Council of Turkey (TÜBİTAK) (Project No. MFAG-114F192). Some of the calculations for this project were carried out using the computing facilities on the Intel Nehalem (i7) cluster (ceres) in the School of Physics, University of Exeter, United Kingdom.

- 
- [1] R. Nagarajan, E. V. Sampathkumaran, L. C. Gupta, R. Vijayaraghavan, V. Prabhawalkar, Bhaktidarshan, and B. D. Padalia, *Phys. Lett. A* **84**, 275 (1981).
  - [2] E. V. Sampathkumaran, G. Wortmann, and G. Kaindl, *J. Magn. Magn. Mater.* **54–57**, 347 (1986).
  - [3] W. Jeitschko, R. Glaum, and L. Boonk, *J. Solid State Chem.* **69**, 93 (1987).
  - [4] M. Rotter, M. Tegar, and D. Johrendt, *Phys. Rev. Lett.* **101**, 107006 (2008).
  - [5] M. Reehuis, W. Jeitschko, M. H. Moller, and P. J. Brown, *J. Phys. Chem. Solids* **53**, 687 (1992).
  - [6] J. An, A. S. Sefat, D. J. Singh, and Mao-Hua Du, *Phys. Rev. B* **79**, 075120 (2009).
  - [7] Yu-Zhong Zhang, H. C. Kandpal, I. Opahle, H. O. Jeschke, and R. Valenti, *Phys. Rev. B* **80**, 094530 (2009).
  - [8] H. Fujii and A. Sato, *Phys. Rev. B* **79**, 224522 (2009).
  - [9] N. H. Sung, Jong-Soo Rhyee, and B. K. Cho, *Phys. Rev. B* **83**, 094511 (2011).
  - [10] J. W. Wang I. A. Chen, T. L. Hung Y. B. You, H. C. Ku, Y. Y. Hsu, J. C. Ho, and Y. Y. Chen, *Phys. Rev. B* **85**, 024538 (2012).
  - [11] T. L. Hung, I. A. Chen, C. H. Huang, C. Y. Lin, C. W. Chen, Y. B. You, S. T. Jian, M. C. Yang, Y. Y. Hsu, J. C. Ho, Y. Y. Chen, and H. C. Ku, *J. Low Temp. Phys.* **171**, 148 (2013).
  - [12] T. Samuely, J. G. Rodrigo, N. H. Sung, B. K. Cho, and P. Samuely, *J. Supercond. Nov. Magn.* **26**, 1199 (2013).
  - [13] V. K. Anand, H. Kim, M. A. Tanatar, R. Prozorov, and D. C. Johnston, *Phys. Rev. B* **87**, 224510 (2013).
  - [14] I. R. Shein and A. L. Ivanovskii, *Physica B* **405**, 3213 (2010).
  - [15] D. S. Jayalakshmi and M. Sundareswari, *J. Alloys Compd.* **561**, 268 (2013).

- [16] M. A. Ghebouli, A. Bouhemadou, B. Ghebouli, M. Fatmi, and S. Bin-Omran, *Solid State Commun.* **151**, 976 (2011).
- [17] I. R. Shein, S. L. Skornyakov, V. I. Anisimov, and A. L. Ivanovskii, *J. Supercond. Nov. Magn.* **27**, 155 (2014).
- [18] A. Subedi and D. J. Singh, *Phys. Rev. B* **78**, 132511 (2008).
- [19] F. Ronning, N. Kurita, E. D. Bauer, B. L. Scott, T. Park, T. Klimczuk, R. Movshovich, and J. D. Thompson, *J. Phys.: Condens. Matter* **20**, 342203 (2008).
- [20] P. Giannozzi, S. Baroni, N. Bonini, M. Calandra, R. Car, C. Cavazzoni, D. Ceresoli, G. L. Chiarotti, M. Cococcioni, I. Dabo, A. D. Corso, S. de Gironcoli, S. Fabris, G. Fratesi, R. Gebauer, U. Gerstmann, C. Gougoussis, A. Kokalj, M. Lazzeri, L. Martin-Samos, N. Marzari, F. Mauri, R. Mazzarello, S. Paolini, A. Pasquarello, L. Paulatto, C. Sbraccia, S. Scandolo, G. Sclauzero, A. P. Seitsonen, A. Smogunov, P. Umari, and R. M. Wentzcovitch, *J. Phys.: Condens. Matter* **21**, 395502 (2009).
- [21] A. B. Migdal, *Zh. Eksp. Teor. Fiz.* **34**, 1438 (1958).
- [22] G. M. Eliashberg, *Sov. Phys. JETP* **11**, 696 (1960).
- [23] P. B. Allen and R. C. Dynes, *Phys. Rev. B* **12**, 905 (1975).
- [24] W. Kohn and L. J. Sham, *Phys. Rev.* **140**, A1133 (1965).
- [25] J. P. Perdew, K. Burke, and M. Ernzerhof, *Phys. Rev. Lett.* **77**, 3865 (1996).
- [26] R. Stumpf, X. Gonge, and M. Scheffler, *A List of Separable, Norm-conserving, Ab Initio Pseudopotentials* (Fritz-Haber-Institut, Berlin, 1990).
- [27] H. J. Monkhorst and J. D. Pack, *Phys. Rev. B* **13**, 5188 (1976).
- [28] S. Bağcı, H. M. Tütüncü, S. Duman, and G. P. Srivastava, *Phys. Rev. B* **81**, 144507 (2010).
- [29] E. D. Mun, S. L. Bud'ko, N. Ni, A. N. Thaler, and P. C. Canfield, *Phys. Rev. B* **80**, 054517 (2009).
- [30] D. Kasinathan, A. Ormeci, K. Koch, U. Burkhardt, W. Schnelle, A. Leithe-Jasper, and H. Rosner, *New J. Phys.* **11**, 025023 (2009).
- [31] H. Hiramatsu, T. Kamiya, M. Hirano, and H. Hosono, *Physica C* **469**, 657 (2009).
- [32] D. C. Johnston, *Adv. Phys.* **59**, 803 (2010).
- [33] L. Ortenzi, S. Biermann, O. K. Anderson, I. I. Mazin, and L. Boeri, *Phys. Rev. B* **83**, 100505(R) (2011).
- [34] A. Subedi, *Phys. Rev. B* **92**, 174501 (2015).